Exploring the Impact of Ischemic Stroke on Brain Function: Insights from Functional Connectivity Gradients and Temporal Lag Correction

Cemal Koba[1,*], Joan Falcó-Roget[1], and Alessandro Crimi[1,2]

[1]Sano Centre for Computational Medicine, Computer Vision Team, Kraków, Poland
[2]AGH University of Krakow, Kraków, Poland
[*]Correspondence: c.koba@sanoscience.org

ABSTRACT

This study investigates the impact of acute ischemic stroke on brain functional organization and evaluates the influence of temporal lag correction on connectivity gradients. Ischemic stroke disrupts blood flow, leading to functional and structural changes associated with behavioral deficits. We investigated stroke-related functional differences via gradients approach, which is useful to examine the macroscale functional organization of the brain. We identified significant functional deviations primarily within somatomotor, visual, and ventral attention networks, correlating with behavioral impairments. These deviations are more pronounced in regions proximal to the lesion, particularly within the right hemisphere, suggesting its heightened vulnerability. Additionally, we observed negative correlations between functional deviation and left motor, spatial memory, and visual bias performance. Temporal lag correction significantly alters gradient values, particularly along the superior-inferior axis, enhancing alignment with the temporal domain. Stroke subjects benefit notably from this correction, with pronounced differences observed in the visual-somatomotor gradient. Overall, this study underscores the utility of connectivity gradients in delineating stroke-related functional alterations and highlights the importance of temporal lag correction in gradient calculation.

Introduction

Ischemic stroke occurs when a vessel supplying blood to the brain is obstructed, ultimately leading to blood shortage (Roach et al., 2010). Lack of blood flow, even for a short time, causes abnormal neural dynamics. If it lasts long enough, neural death is unavoidable. The region that suffers from the lack of blood flow will be infarcted, and there is a chance that the surrounding region will be swollen (J. M. Hong et al., 2021). These changes in the brain's structure are associated with a wide range of behavioral and neural dysfunctions, not only within the lesion site but also in its anatomically and functionally connected areas. Motor, linguistic, and attention-related behavioral deficits are commonly observed in stroke patients (He et al., 2007; Siegel, Ramsey, et al., 2016). Task and resting-state (RS) activity and networks that are related to those functions are therefore subject to change. During arm-moving tasks, the contralateral hemisphere shows over-activity (Rehme et al., 2011). This over-activity decreases with the recovery time. RS studies showed that the behavioral deficits are related to the decrease in the connectivity of their respective pre-defined network (e.g. motor dysfunction and motor network - Carter et al., 2010, attention performance with attention network - Corbetta and Shulman, 2002). The decreases show the difference between intact and damaged hemispheres (Carter et al., 2010). In general, decreased overall connectivity between hemispheres, and increased overall connectivity within the contralateral hemispheres to lesions are observed (New et al., 2015; Yourganov et al., 2021). This difference in lateralization is also reported via homotopic connectivity. Decreased connectivity between homotopic regions of stroke subjects between intact and damaged hemispheres has been related to the lesion size and severity (Tang et al., 2016; Urbin et al., 2014). Lastly, the network-based approach is also a useful method for reporting stroke-related differences. Altered nodal degrees in the default mode network were found for stroke patients (Zhu et al., 2017). In addition, damage to connector hubs seems to make the most of the connectivity difference (Gratton et al., 2012).

The effect of stroke on brain function and structure varies depending on the extent and the location of the lesion, making it difficult to make group-level inferences on pre-defined resting-state (RS) networks. However, studies with large sample sizes show that the occurrence of the ischemic stroke is not random (Thiebaut de Schotten et al., 2020; Weaver et al., 2019). The most common regions that are affected by ischemic stroke are basal ganglia, cerebrospinal tract, and cerebellum. Considering this dichotomy of the individual and sample characteristics, dimension reduction techniques, such as functional connectivity gradients (Margulies et al., 2016; Vos de Wael et al., 2020) may help in understanding the consequences of stroke from a more general point of view, as it displays the macroscale functional organization, rather than discrete and specific characteristics of the connectivity such as functional connectivity of regions or network-based statistics. The connectivity gradients approach

shows the major axes of the brain's functional organization. The most dominant axis is organized from unimodal to transmodal functions, meaning that brain function can be explained mainly by these two sides of the same gradient. Following the first one, the second gradient indicates sensorimotor-visual functions, and the third gradient shows active-passive attention. The gradients of brain function are highly replicable (Bethlehem et al., 2020; Hardikar et al., 2022; S.-J. Hong et al., 2019; Margulies et al., 2016; Mckeown et al., 2020) .

Differences in gradient scores (indicating a region's position on the functional gradient) proved to show meaningful differences in the functional organization of clinical groups (autism - S.-J. Hong et al., 2019, depression - Xia et al., 2022). Further metrics that can be derived from the gradients are related to the 3D distribution of the functional organization, such as gradient range and variation (Del Río et al., 2022), dispersion (distance of each node to the centroid of the network, Valk et al., 2023) and eccentricity (distance of each node to the centroid of the coordinate system Valk et al., 2023). Among the studies that explore brain organization via connectivity gradients, only one study used stroke patients as the subject of interest (Bayrak et al., 2019). The authors used "functional distance to lesion" as a metric, which is the similarity between the gradient score of any given point on the brain and the lesion area. They reported that this metric and functional connectivity stability over time are related. The closer a region is to the lesion on functional space, the more unstable it is. This relationship was reported for the 1st and the 3rd gradients.

Apart from the heterogeneity of the stroke lesions at the individual level, another concerning issue for stroke research is the difference in the blood oxygen level-dependent (BOLD) signal from the lesioned areas. By description is ischemic stroke, the BOLD signal, which is dependent on blood flow, shows different temporal characteristics compared to that of healthy tissue during both task and resting state fMRI. To exemplify, the BOLD of stroke patients showed later peak values (Altamura et al., 2009; Bonakdarpour et al., 2015), and are in a lower frequency domain (Siegel, Snyder, et al., 2016). Recent advancements in fMRI techniques showed that it is possible to detect stroke lesions via perfusion maps that are created solely from BOLD data. This technique calculates the time lag between a voxel and a reference time series (e.g. global signal - GS, or venous sinuses) (Braban et al., 2023; Khalil et al., 2020; Lv et al., 2013; Tong et al., 2017). The lag maps highlight the areas with delayed blood flow, hence the lesioned areas. Correcting the RS data for these time lags increased the strength of the functional connectivity, assuming that the lesioned areas become more comparable with non-lesioned areas (Siegel, Snyder, et al., 2016). The time lag is thought to be resourced from the lack of blood flow in the lesioned areas. However, even after correction, the relationship between behavioral dysfunction and functional connectivity metrics persists (Siegel, Snyder, et al., 2016). When this method is applied to healthy subjects, a degree of improvement in the data quality is observed (Erdoğan et al., 2016). This step aligns the data on the temporal domain, eliminating the temporal differences caused by the blood flow. In addition, Tong et al. (2019) discuss that delay maps also contain noise from very low-frequency oscillations such as cardiac and respiratory signals, therefore correcting for them improves the functional connectivity for the healthy controls.

In this study, the effect of ischemic stroke on the macroscale functional organization and the effect of temporal lag correction on the functional connectivity gradients are explored. Thanks to the 3D organization derived from the connectivity gradients, stroke subjects are expected to have larger deviations compared to control subjects. The deviations in 3D space are expected to be related to the structural and behavioral measures. Considering the previous reports on the hemispheric differences in the case of acute ischemic stroke, a hemispheric difference in the deviation is expected. Lastly, correction for the time lag is expected to improve the gradient distribution, more so for stroke patients. After the lag correction, the remaining difference is expected to reflect the difference due to function, rather than the difference in the metabolic differences.

Methods

Dataset details

The dataset was collected by the School of Medicine of the Washington University in St. Louis and complete procedures can be found in Corbetta et al., 2015. They collected MRI data and behavioral examinations of stroke patients and healthy controls. Stroke patients were registered according to the following criteria:

- The subject must be older than 18 years of age,
- The subject must have no history of stroke until the current one,
- The stroke must have up to two lacunes, be clinically silent, be less than 15 mm in size on CT scan,
- Clinical evidence for motor, language, attention, visual, or memory deficits based on neurological examination,
- The onset of stroke must be shorter than 2 weeks during the time of the scan,
- The subject must be awake, alert, and capable of participating in research.

The imaging data consists of structural and functional MRI at three different time points for stroke patients (1-2 weeks, 3 months, and 12 months after stroke), and 2 time points for control patients (initial scan and 3 months later). Structural scans

include T1-weighted, T2-weighted, and diffusion tensor images. Functional images include a resting state paradigm. Scanning was performed with a Siemens 3T Tim-Trio scanner at the School of Medicine of the Washington University in St. Louis including structural, functional, and diffusion tensor scans. Structural scans consisted of (1) a sagittal MP-RAGE T1-weighted image (TR=1950 msec, TE=2.26 msec, flip angle=9 deg, voxel size=1.0 x 1.0 x 1.0 mm, slice thickness = 1.00 mm); (2) a transverse turbo spin-echo T2-weighted image (TR=2500 msec, TE=435 msec, voxel-size=1.0 x 1.0 x 1.0 mm, slice thickness = 1.00 mm); and (3) a sagittal FLAIR (fluid-attenuated inversion recovery) (TR=7500 msec, TE=326 msec, voxel-size=1.5 x 1.5 x 1.5 mm, Slice thickness = 1.50 mm). Functional images consisted of 1-7 resting state runs for each session (TR=2000 msec, TE=27 msec, voxel-size= 4 x 4 x 4 mm, slice thickness = 4 mm, total duration = 256 seconds for each run).

Preprocessing of the imaging data

The dataset was received in DICOM format. Conversion from DICOM to NIFTI format was achieved by an in-house script that operates on Python (Falcó-Roget, 2023). The files were then organized according to the BIDS specifications. In this step, sessions with duplicate scans (back-to-back scanning of any modality) were manually checked by two independent researchers (C.K., J.F.-R.). Scans with lower quality were discarded from future analyses after visual inspection. Multiple scanning happened only when the first acquisition had low quality. Runs that had no T1 or RS scan were removed. Additionally, some RS scans were identical, labeled as *"motion reference/moco"*, and removed. The dataset consisted of hemorrhagic and ischemic stroke cases. Only the ischemic stroke cases of the acute scans were kept.

The dataset (organized in BIDS format, bad quality / duplicate scans removed), was preprocessed with *fmriprep* (Esteban et al., 2019) on a supercomputer using *Apptainer* (formerly known as *Singularity*, Kurtzer et al., 2017).

Results included in this manuscript come from preprocessing performed using *fMRIPrep* 23.1.3 (Esteban et al. (2019); Esteban et al. (2018); RRID:SCR_016216), which is based on *Nipype* 1.8.6 (K. Gorgolewski et al. (2011); K. J. Gorgolewski et al. (2018); RRID:SCR_002502).

Anatomical data preprocessing

The T1-weighted (T1w) images were corrected for intensity non-uniformity (INU) with `N4BiasFieldCorrection` (Tustison et al., 2010), distributed with ANTs (Avants et al., 2008, RRID:SCR_004757), and used as T1w-reference throughout the workflow. The T1w-reference was then skull-stripped with a *Nipype* implementation of the `antsBrainExtraction.sh` workflow (from ANTs), using OASIS30ANTs as target template. Brain tissue segmentation of cerebrospinal fluid (CSF), white-matter (WM) and gray-matter (GM) were performed on the brain-extracted T1w using `fast` (FSL, RRID:SCR_002823, Zhang et al., 2001). Volume-based spatial normalization to one standard space (MNI152NLin2009cAsym) was performed through nonlinear registration with `antsRegistration` (ANTs), using brain-extracted versions of both T1w reference and the T1w template. *ICBM 152 Nonlinear Asymmetrical template version 2009c* [Fonov et al. (2009), RRID:SCR_008796; TemplateFlow ID: MNI152NLin2009cAsym] template was selected for spatial normalization and accessed with *TemplateFlow* (23.0.0, Ciric et al., 2022).

Functional data preprocessing

For each of the BOLD runs found per subject (across all runs), the following preprocessing was performed. First, a reference volume and its skull-stripped version were generated using a custom methodology of *fMRIPrep*. Head-motion parameters with respect to the BOLD reference (transformation matrices, and six corresponding rotation and translation parameters) are estimated before any spatiotemporal filtering using `mcflirt` (*FSL* , Jenkinson et al., 2002). BOLD runs were slice-time corrected 0.5 of slice acquisition range using `3dTshift` from *AFNI* (Cox & Hyde, 1997, RRID:SCR_005927). The BOLD time-series (including slice-timing correction when applied) were resampled onto their original, native space by applying the transforms to correct for head-motion. These resampled BOLD time-series will be referred to as *preprocessed BOLD in original space*, or just *preprocessed BOLD*. The BOLD reference was then co-registered to the T1w reference using `mri_coreg` (*FreeSurfer*) followed by `flirt` (*FSL* , Jenkinson & Smith, 2001) with the boundary-based registration (Greve & Fischl, 2009) cost-function. Co-registration was configured with six degrees of freedom. Several confounding time-series were calculated based on the *preprocessed BOLD*: framewise displacement (FD), DVARS and three region-wise global signals. FD was computed using two formulations following Power (absolute sum of relative motions, Power et al. (2014)) and Jenkinson (relative root mean square displacement between affines, Jenkinson et al. (2002)). FD and DVARS are calculated for each functional run, both using their implementations in *Nipype* (following the definitions by Power et al., 2014). The three global signals are extracted within the CSF, the WM, and the whole-brain masks. The head-motion estimates calculated in the correction step were also placed within the corresponding confounds file. The confound time series derived from head motion estimates and global signals were expanded with the inclusion of temporal derivatives and quadratic terms for each (Satterthwaite et al., 2013). The BOLD time-series were resampled into standard space, generating a *preprocessed BOLD run in MNI152NLin2009cAsym space*. First, a reference volume and its skull-stripped version were generated using a custom methodology of *fMRIPrep*. All resamplings can be performed with *a single interpolation step* by composing all the pertinent

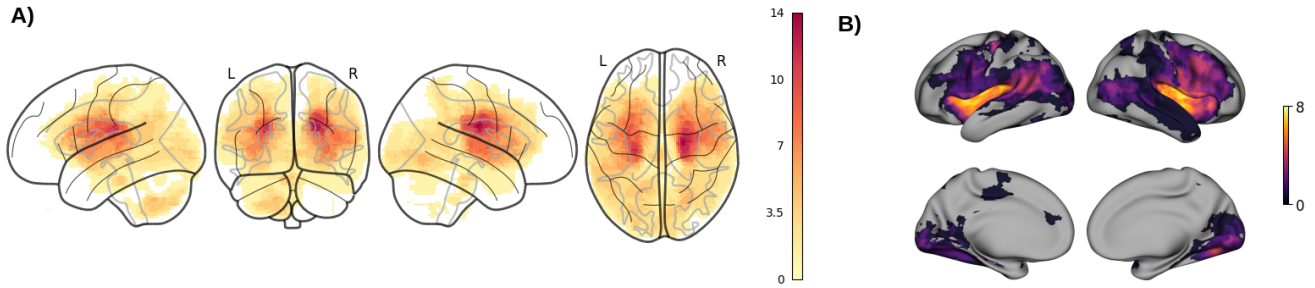

Figure 1. Profiles of ischemic stroke occurrence. A) Overlap of the 84 manually drawn lesion masks in the subcortical and cerebellar areas. Regions around the basal ganglia and thalamus show the most overlap, especially in the right hemisphere. The colorbar shows the number of subjects. **B)** Cortical projection of the lesion occurrences. Total number of subjects with cortical lesion occurrence is less than the total number of subjects with subcortical lesion occurrence.

transformations (i.e. head-motion transform matrices, susceptibility distortion correction when available, and co-registrations to anatomical and output spaces). Gridded (volumetric) resamplings were performed using `antsApplyTransforms` (ANTs), configured with Lanczos interpolation to minimize the smoothing effects of other kernels (Lanczos, 1964). Non-gridded (surface) resamplings were performed using `mri_vol2surf` (FreeSurfer).

Many internal operations of *fMRIPrep* use *Nilearn* 0.10.1 (Abraham et al., 2014, RRID:SCR_001362), mostly within the functional processing workflow. For more details of the pipeline, see the section corresponding to workflows in *fMRIPrep*'s documentation.

Copyright Waiver: The above boilerplate text was automatically generated by *fMRIPrep* with the express intention that users should copy and paste this text into their manuscripts *unchanged*. It is released under the CC0 license.

Following a quality control of *fMRIPrep* outputs, 26 control subjects and 104 stroke subjects were qualified for further analysis. Each subject had 1-7 R S runs (112 subjects with 7 runs, 9 subjects with 6 runs, 4 subjects with 5 runs, 4 subjects with 3 runs, and 2 subjects with 2 runs), in total of 875 runs for 130 subjects. Among 104 stroke subjects, 84 of them had manually drawn lesion masks available in the dataset. Regions that are most often damaged were the subcortical area, covering the thalamus and basal ganglia (Figure 1).

Outputs of *fMRIPrep* were further cleaned from nuisance regressors using a custom script written in MATLAB. The 36P strategy without GS regression that is described in Satterthwaite et al. (2013) was adopted to choose the regressors of no interest. Specifically, 6 motion regressors, mean signal from white matter and CSF, their first derivatives, power, and power of the first derivatives were chosen. In addition, mean frame-wise displacement and a linear trend were added to the model. These regressors were removed from the fMRI data using a multiple linear regression model and the residuals were saved. A band-pass filter between 0.01-0.1 was applied to the residuals.

Calculating the functional connectivity gradients and the reference topography

Mean time series from GM were calculated using an improved version of the Schaefer-Yeo atlas that parcellates the cortex into 400 regions across 7 functional networks (Glen et al., 2021; Schaefer et al., 2018). The averaged time series were then correlated with each other, resulting in 400 x 400 correlation matrices for each run of each subject. Average correlation matrices across runs were calculated and normalized via Fisher's Z transformation. This step generated one correlation matrix for each subject.

Functional connectivity gradients based on the correlation matrices were generated as described in Margulies et al. (2016) using the available functions in the *BrainSpace* MATLAB toolbox (Vos de Wael et al., 2020). In short, correlation matrices were thresholded to keep the top 10% of the connections. The normalized angle similarity of the sparse matrices was calculated. A non-linear dimension reduction technique, diffusion mapping, was applied to the similarity matrices with an alpha value of 0.5 for the manifold. This step generated 10 gradient values that explain the functional connectivity profile of each ROI and for each subject. Lastly, Procrustes alignment was used on the gradients to make them comparable. Since diffusion mapping can result in values in the opposite directions, a reference gradient computed based on the correlation matrix that came with *BrainSpace* was used. This procedure generated "gradient scores" that show the position of each region for 10 gradients. Only the scores of the first three gradients were kept for the following analyses.

In stroke patients, lesion lateralization is known to play an important role in behavioral and cognitive impairments. To study the functional connectivity profiles in intact and lesioned hemispheres independently we computed the connectivity gradients for intrahemispheric connections using the same methods. Importantly, participants with lesions on the left side ($n = 56$) and

on the right ($n = 48$) were treated separately, and intrahemispheric subsets of the (400×400) matrices were extracted for each patient. Intact and lesioned hemispheric functional connectivity gradients were then computed based on the similarity profiles of the (200×200) functional connections.

Euclidean distance to the reference topography

The first 3 gradients ($\mathbf{G1}, \mathbf{G2}, \mathbf{G3}$) constitute the orthogonal axes of a Euclidean space (i.e., 3D space) where the functional topography can be embedded. One of the main advantages of this approach is the considerably lower number of dimensions present in the data. Since this space is normed, we defined the position in this latent space as $\mathbf{x}_{s,r} = (G1_{s,r}, G2_{s,r}, G3_{s,r})$ for each subject s and ROI r. Then, for each ROI, a reference 3D organization was created by averaging the distribution over all control subjects N_{C_s}, $\hat{\mathbf{x}}_r = \frac{1}{N_{C_s}} \sum_{s=1}^{N_{C_s}} \mathbf{x}_{s,r}$ (which will be referred as reference topography). The Euclidean distance (ED) to the reference topography was calculated for every control and stroke subject as the $L2$ norm of the difference between the ROI's and the reference positions, $\mathrm{ED}_{func} = ||\mathbf{x}_{s,r} - \hat{\mathbf{x}}_r||$. The ED to the 3D reference topography will be referred to as ED_{func}, and was calculated using MATLAB's *norm* function.

The mean ED_{func} across all subjects was calculated. This step generated 400 ED_{func} values for control and stroke groups separately. The mean ED_{func} values were compared via a two-sample t-test in order to check if both groups have equal mean distance to reference topography. The significance of the region-wise distances was calculated via a permutation procedure. The mean ED_{func} of the stroke group was subtracted from that of the control group, leaving a vector of 400 differences (one difference value for each ROI). The same difference vector was calculated 10000 times after randomly shuffling the group labels, calculating the mean ED_{func} for each group. This procedure created a null distribution of difference values for each ROI. The value of the real difference of an ROI was considered significant if its absolute value exceeded the 95th percentile value of its null distribution. To detect the source of the difference in ED_{func}, 1 dimensional (1D) ED_{func} for every one of the three gradients was also calculated separately and compared across groups following the same procedure.

Relationship between ED and behavioral-structural measures

The behavioral examination includes five main batteries that consist of various tests (the full list of tests is available in Corbetta et al., 2015). These batteries measure the performance of the motor, linguistic, executive function, memory, and attentional capabilities. It was shown that multiple tests could be clustered into a reduced set of factors to account for a large variance of functional abnormalities (Corbetta et al., 2015). Three big clusters were identified to account for 60% variance in the behavioral performances. The first big cluster accounted for 25% of the variance and consisted of language, verbal memory, and spatial memory performances. The second big cluster explained 23% of the variance and consisted of visual field bias, left body, and spatial memory factors. Lastly, The third big factor explained 17% of the variance and consisted of right body and attention shifting factors. For each one of the aforementioned domains, we considered the clustered factor as a sufficient predictor of the given behavioral deficit. ED_{func} was correlated with the big cluster scores to investigate the relationship between functional and behavioral abnormalities.

Anatomical ED to lesion (ED_{anat}) was calculated for each subject whose lesion masks were available. After resampling the lesion masks to the resolution of the functional scans, coordinates of the voxels that are marked as "lesioned" were extracted using AFNI's *3dmaskdump*. Then ED between a voxel in the parcellation map and every lesioned voxel was calculated. The minimum distance to the lesioned voxels was defined as the distance to the lesion. This procedure was repeated for every voxel in the parcellation mask. Correlation between ED_{anat} and ED_{func} were calculated for each region was calculated.

To examine the effect of lesion location on the functional deviation, the Jaccard similarity index (JI) between lesion masks of each subject and the correlation between their ED_{func} values were calculated. This step created 83 JI values and 83 correlation coefficients for each subject (there are 84 subjects with lesion masks). The values across subjects were pooled together, resulting in 3486 JI and correlation values. The correlation between the two sets was examined to investigate the similarity between lesion location and functional deviation patterns. The analysis was repeated with ED between centroids of the lesion masks ($\mathrm{ED}_{centroid}$) instead of JI, in case of 0 overlap between the masks.

Differences between intact and damaged hemispheres

To examine how the functional reorganization differs in the right and left hemispheres in the case of lesion or no lesion, the above analyses were repeated using the gradients generated by intrahemispheric connectivity matrices. Specifically, 3D and 1D ED_{func} for right and left hemispheres were compared within intact and damaged hemispheres. Out of 130 subjects, 48 subjects had right hemisphere damage, and 56 subjects had left hemisphere damage. The mean ED_{func} across all subjects were compared between the right and left hemispheres.

Effect of lag correction on the gradients

The time lag of the BOLD signal was calculated in relation to the global signal (GS). GS was derived from the GM mask (whole-brain GM mask for controls, and only the intact hemisphere for the stroke subjects) For each voxel on the cortex, a

correlation with the BOLD signal and the time-shifted version of the GS signal between $\pm$ 3 TR was calculated. The time-shift value that corresponds to the maximum correlation was accepted as the time lag. The BOLD signal was then shifted to that many TRs to correct for the time lag.

400×400 correlation matrices were generated from the corrected time series using the same procedure for the non-corrected time series. We used the functional connectivity aberrancy to measure the effect of this correction (Siegel, Snyder, et al., 2016). This method calculates the Z score of each node in the individual correlation matrices in reference to the mean of the control subjects. For each subject (both control and stroke groups), mean aberrancy across the whole matrix was calculated. These mean values of groups were compared via a two-sample t-test before and after lag correction.

The correlation matrices were then used to generate the functional connectivity gradients as was done for the non-corrected data. Gradient scores of each ROI were compared before and after lag correction within and between groups. All the calculations related to ED_{func} and on whole brain or separate hemispheres were repeated with the lag-corrected gradients as well. The differences between the results of before and after lag correction analyses were compared.

The visualizations in this paper were generated using functions from *BrainSpace* (Vos de Wael et al., 2020), *BrainStat* (Worsley et al., 2009), *SurfPlot* (Gale et al., 2021), and adaptation of code from Bayrak (2019).

Results

Demographics and quality control measures

No difference was found between the mean ages of the groups (number of control subjects = 26, mean age = 55.3 $\pm$ 12.94, number of stroke subjects = 104, mean age = 53.5 $\pm$ 10.73; $t(128) = 0.73$, $p = 0.46$) and sex distribution (stroke subjects = 54 male/50 female, control subjects = 16 male/10 female; $\chi^2 = 1.01$, $p = 0.3$).

Mean FD was higher in control subjects ($t(128) = 4.81$, $p < 0.01$). Variance and maximum values of FD did not show any difference between groups (Supplementary Figure 1).

Connectivity gradients

Functional connectivity gradients revealed the functional similarity profile of the regions depending on how much variance they explain. On average, the first three gradients (G1, G2, G3) explained approximately 40% of the total variance for both groups (16%, 13%, and 10%, respectively, Supplementary Figure 2). The following analyses were conducted on these gradients. There were no differences in the explained variance of the gradients between groups (explained variances for each gradient were compared via two-sample t-test, $p > 0.05$ for 10 gradients, corrected with false-discovery rate - FDR). The principal gradient G1 showed that brain activity is maximally organized between the unimodal/transmodal cortices. The second axis, or G2, showed the visual/sensorimotor regions, and G3 showed the visual-default mode/dorsal attention-frontoparietal for both control and stroke subjects (Figure 2A). For each RS network, ROI-wise gradient scores in controls and patients were found to be statistically equivalent ($p > 0.05$, t-test, corrected with FDR). These results suggest that the functional topography remains largely unaltered in the early stages after the stroke occurs.

Euclidean distance to functional organization

Mean 3D distribution to reference topography (ED_{func}) was calculated for every ROI and every subject. The values of control and stroke subjects were compared via a two-tailed between-samples t-test. The results showed that stroke patients have significantly more mean ED_{func} compared to control subjects ($t(798) = -10.1$, $p < 0.001$). The permutation test and the 7 networks decomposition revealed that the source of the difference is the somatomotor and ventral attention networks, more visible in the right hemisphere (Figure 3). Comparison 1D ED_{func} that were derived from each gradient separately shows that all 3 gradients contribute to this difference (T-stats of the G1, G2, G3: -3.63, -7.9, -6.0, respectively, p-values are smaller than 0.01, Supplementary Figure 3). All 3 gradients showed high mean differences in the somatomotor network. In addition, G2 showed a high difference in the visual network and G3 showed a difference in the ventral attention and limbic networks. Taken together, stroke subjects showed larger functional deviation to the reference topography, specifically in somatomotor, ventral attention, and visual networks. All three gradients showed deviation in the somatomotor network.

Relationship between ED and behavioral-structural measures

Among the 3 big clusters of behavioral scores, only the second big cluster, which is driven by visual field bias and left body performance showed significant correlations with ED_{func} ($n = 42, p < 0.05$, corrected via FDR. Mean correlation across 32 significant regions: -0.52 $\pm$ 0.06, Figure 4). Regions that show the highest correlation were from sensorimotor, ventral attention, and default mode networks, mainly on the right hemisphere. Although the other two factors showed consistent patterns, their results did not survive FDR correction. Similarly, the correlation between ED_{func} and ED_{anat} showed a negative relationship in sensorimotor and control networks (Supplementary Figure 5). The correlation between ED_{func} and behavioral-structural measures are the strongest on the right sensorimotor regions. However, the results did not survive FDR correction as well.

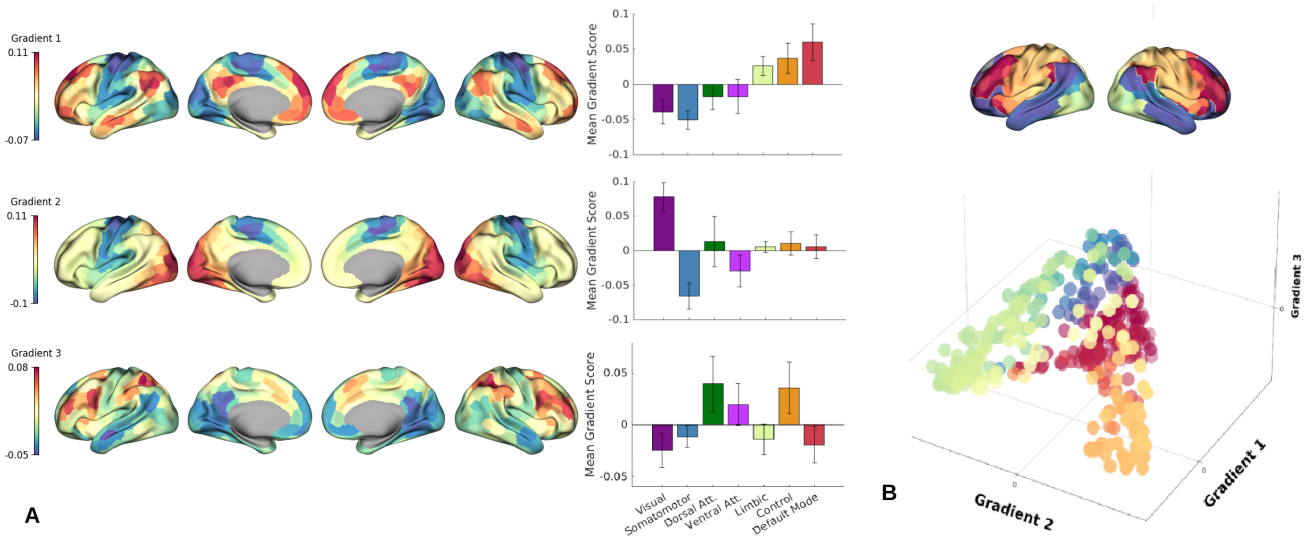

Figure 2. Reference topography from control subjects. A): Projection of the mean gradient scores on the surface meshes (left) and their decomposition by 7 networks (right). Error bars depict 1 Standard Error of the Mean (SEM). **B)**: Reference topography in 3D space, and its projection on a surface mesh.

The correlation between JI, $\mathrm{ED}_{centroid}$, and ED_{func} showed ED_{func} and $\mathrm{ED}_{centroid}$ are weakly correlated ($r = -0.04, p < 0.05$). The correlation becomes stronger when the subjects with right hemisphere damage are considered only ($r = -0.12, p < 0.005$), and disappears for the subjects with left hemisphere damage ($r = -0.03, p > 0.05$). The center of the lesion is weakly related to similar functional deviation patterns when the damage is on the right hemisphere (Table 1).

Differences between intact and damaged hemispheres

Damaged hemispheres showed no ED_{func} difference (3D ED_{func} $t(398) = -0.06$, $p = 0.94$). For reference, the right and left hemispheres of the control subjects were also compared ($t(398) = -0.70$, $p = 0.48$). The comparison between the ED_{func} of the intact right and left hemispheres to their corresponding control distribution in 3D space showed a higher mean ED_{func} value in the right hemisphere ($t(398) = -3.43, p = 0.0006$). Repeating the same analysis by using the ED_{func} of each 3-gradient separately showed that the difference is specific to the second gradient (Difference for the 1st, 2nd, and 3rd gradients respectively: $t(398) = -0.88, -2.39, -1.61$, $p = 0.37, 0.01, 0.11$). Relaying the mean distance on the surface showed that the highest difference on the 2nd gradient is placed on the visual and sensorimotor areas (Supplementary Figure 4).

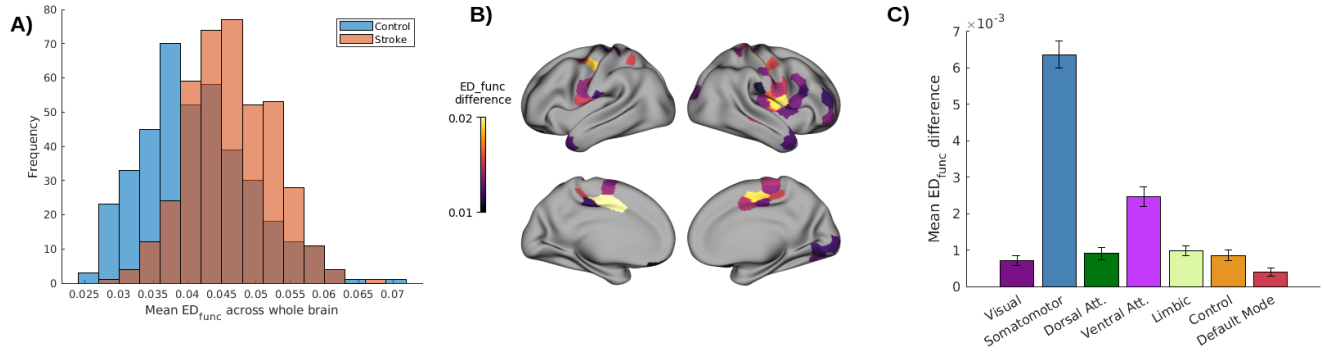

Figure 3. ED_{func} difference between control and stroke subjects. A) Histogram of ED_{func} between control and stroke subjects. **B)** Significant region-wise 3D ED_{func} differences ($p < 0.05$, permutation test). All the differences favor stroke subjects, meaning that the ED_{func} is larger in the stroke subjects for the given regions. **C)** Differences in ED_{func} across networks [mean $\pm$ SEM].

	All				LH				RH			
JI	1.00				1.00				1.00			
ED_centroid	-0.53***	1.00			-0.40***	1.00			-0.49***	1.00		
ED_func_before	0.03	-0.04*	1.00		0.02	-0.03	1.00		0.08*	-0.12**	1.00	
ED_func_after	0.01	-0.03	0.78	1.00	0.05	-0.01	0.79	1.00	0.02	-0.08*	0.84	1.00

Table 1. Correlation between Jaccard Index (JI), ED between centroids of the lesions ($ED_{centroid}$), and ED_{func} before and after lag correction. across all subjects (All), subjects with right hemisphere damage (RH), and subjects with left hemisphere damage (LH) ($* : p < 0.05, ** : p < 0.005, *** : p < 0.0005$)

Effect of lag correction on the gradients

Mean lag maps in reference to GS showed a pattern on the inferior-superior axis (consistent with Erdoğan et al. (2016) and Tong et al. (2019); Figure 5C-D). The visual cortices have a negative delay, hence behind the GS signal, and somatomotor areas have a positive delay, meaning that they are followed by the GS. Mean, and variance of the lag values did not show any difference between the groups ($t(798) = -0.91, 1.17$, $p = 0.35, 0.24$, respectively). However, maximum lag values were higher in stroke subjects, and minimum lag values were higher in controls ($t(798) = -13.72, 13.47$, respectively, $p < 0.001$ for both, Supplementary Figure 6). In other words, stroke subjects showed more extreme lag values on both sides.

Stroke subjects showed higher functional connectivity aberrancy compared to the control subjects before lag correction (Figure 5A-B). After the correction, there were no differences in terms of the functional connectivity strength between the groups. Also, the mean functional connectivity of both groups was increased after the correction.

ROI-based comparison of the gradient scores before and after lag correction resulted in differences in both groups ($p < 0.05$, corrected with FDR, Figure 6). In control subjects, higher gradient scores in temporal and frontal poles and lower scores on cuneus were observed for G1, higher scores in temporal poles and lower scores in visual cortices were observed for G2, and higher scores in cuneus and superior frontal gyri and lower score for temporal poles, frontal poles, and inferior temporal gyri for G3. For stroke subjects, these patterns were similar but more expanded, with the highest expansion in the second gradient. There was no difference between control and stroke subjects after lag correction, as it was before the lag correction.

Explained variances (scaled eigenvalues) also increased for G1 and G2 in stroke subjects after lag correction ($t(103) = -4.96, -4.61$, respectively, $p < 0.05$, corrected with FDR). The mean explained variance increased by $0.97\% \pm 2$ in G1 and $0.57\% \pm 1.24$ in G2 ($p < 0.05$, corrected with FDR).

3D ED_{func} between control and stroke subjects show the same direction as before correction (higher mean ED_{func} in stroke subjects, $t(798) = -12.05$, $p < 0.001$). The lag correction did not significantly change the result ($t(399) = 1.86$, $p = 0.06$). However, number of significant ROIs increased from 64 to 97, and the pattern preserved its core shape. 1D ED_{func} across 3 gradients give significant differences in favor of stroke subjects as well (T-stats of G1, G2, G3: -4.01, -10.21, -6.31). When compared with 1D ED_{func} before lag correction, only the G2 resulted in a significant difference ($t(399) = 4.63$, $p < 0.001$). The 1D difference in G2 increased the significant regions from 51 to 98. The difference mostly happened in the limbic network (Figure 7).

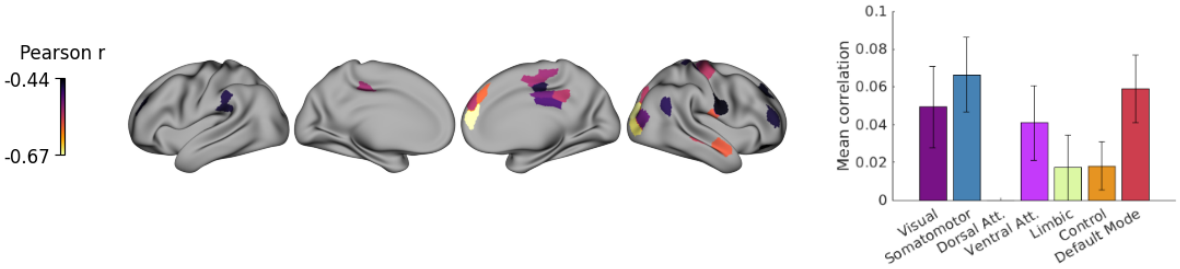

Figure 4. Correlates of behavioral impairment. Regions that show correlation (left) between ED_{func} and big factor 2 and their contribution to the 7 networks (right). After correction for multiple comparison correction via non-parametric permutation procedure. Factor 2 explains visual field bias and left motor performance. There is a negative relationship between behavioral performance and functional deviation. The better the subjects perform in visual field bias and left motor tasks, the less functional deviation they exhibit in those regions.

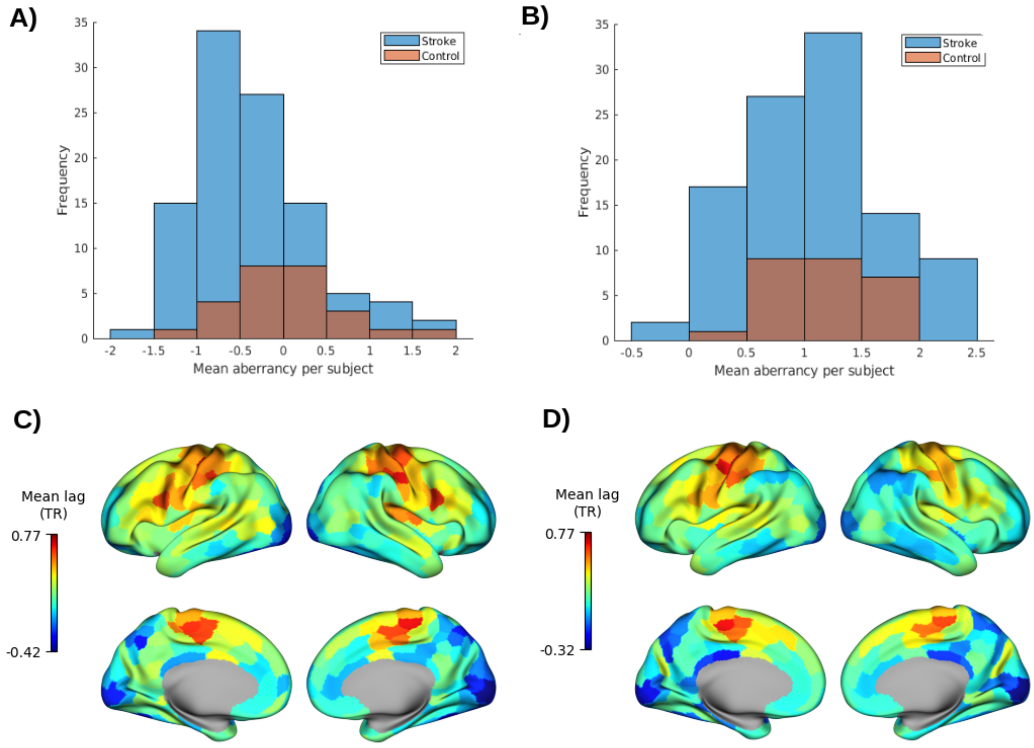

Figure 5. Functional connectivity aberrancy of control and stroke subjects. (A) Before and, **(B)** after lag correction. Aberrancy is calculated in reference to the mean connectivity of control subjects before lag correction. It can be seen that before lag correction, stroke subjects show aberrancy, but after lag correction, the data of the two groups align. The lag patterns of control and stroke groups can be seen in **(C)** and **(D)**, respectively.

Lag correction affected the results of the intrahemispheric gradients from intact and damaged hemispheres as well. The mean ED_{func} difference between left and right intact hemispheres became stronger ($t(398 = -5.72)$, $p < 0.001$, the difference between before and after lag correction: $t(398 = 3.43, p < 0.001)$. As opposed to the non-corrected ED_{func}, corrected ED_{func} in the damaged hemispheres showed a significant difference with right hemisphere showing higher ED_{func} ($t(398 = -2.81)$, $p < 0.001$, the difference before and after lag correction was: $t(398 = 4.47)$, $p < 0.001$).

When correlated with mean gradient scores, the mean lag pattern showed a very high correlation with G2 ($r = 0.7$), and lower with G1 ($r = 0.25$) and G3 ($r = 0.2$, p values < 0.001, FDR corrected).

To capture a similar nuance with ED_{func}, for each subject, the difference between the individual lag value and the mean lag value from control subjects was calculated for each ROI. The mean lag difference was correlated with mean ED_{func}. Control subjects almost zero correlation ($r = 0.02$, $p = 0.6$), whereas stroke subjects showed stronger correlation ($r = 0.2$, $p < 0.001$). The lag correction did not change those values marginally ($r = 0.02$ and 0.21). When checked individually (across the brain, one value per subject), no significant differences between groups were found, and no correlation was found.

When correlated with behavioral measures, both mean lag and lag difference showed very few regions with a p value below 0.05 and did not reveal a meaningful pattern. When the ED_{func} and those behavioral metrics were recalculated after lag calculation, the general patterns were preserved without significant differences in the number of significant ROIs or mean correlation values in the significant ROIs. Similarly, correlation between ED_{func} and ED_{anat} were not affected by lag correction.

Lastly, lag correction affects the relationship between the lesion location and the similarity in ED_{func}. After lag correction, the correlation between the center of lesion masks and the similarity between ED_{func} decreased (Table 1).

Discussion

The first aim of this study was to identify the effect of acute ischemic stroke on the functional organization of the brain. The connectivity gradients were used as a metric because of their ability to decompose the functional connectivity matrices into 3D

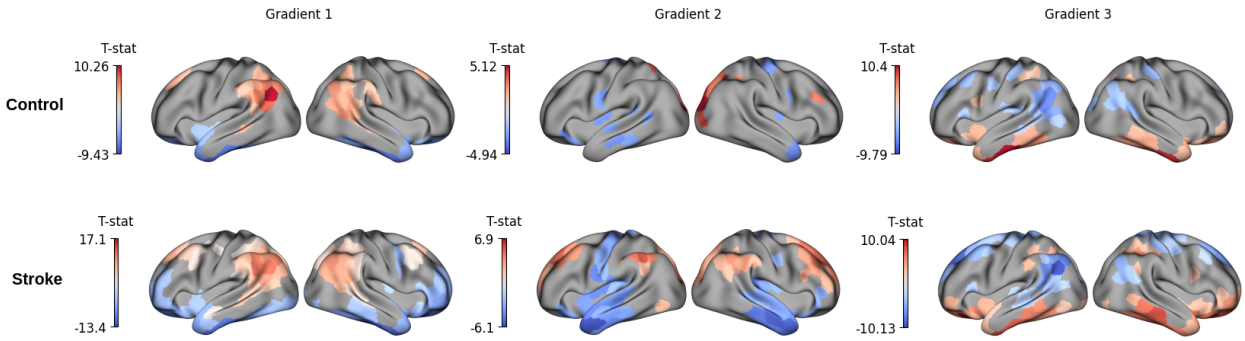

Figure 6. Effect of lag correction on the gradient scores. Gradient scores of each region were compared before and after lag correction via a t-test, and p-values are corrected with FDR. Top row: Control group, Bottom row: Stroke group. Stroke subjects show similar but larger differences in gradient scores after lag correction (colorbars emphasize different ranges for the T statistic).

distribution, which makes it possible to track functional changes in each region of each subject, regardless of the location and the extent of the stroke lesion.

Although the gradient scores did not show any differences at the group level, a comparison of the functional deviation values showed that stroke is related to large functional deviations, primarily in the somatomotor network, followed by the visual and ventral attention networks. The changes related to these networks have been reported before and found related to behavioral dysfunctions such as motor problems, aphasia, and attentional deficits (Carter et al., 2010; Corbetta & Shulman, 2002; He et al., 2007; Siegel, Ramsey, et al., 2016). The functional deviation in our study was correlated to left motor and visual attention performance as well. Considering the consistency with previous reports, it can be said that functional deviation is a good estimator of the impact of the stroke on brain function. Lastly, regions that showed a high correlation with behavioral performances also showed a relationship with anatomical distance to the lesion. The further away they are from the lesion, the less functional deviation they exhibit. Taking all these associations into account, only a set of regions, mainly in the right sensorimotor area, are sensitive to the stroke lesion.

One possible explanation for the concentration of the sensitive regions on the right sensorimotor and ventral attention network could be the higher number of overlapped lesions on the right hemisphere. The pattern of the functional deviation resembles the distribution of the lesions on gray matter. It can be said that functional deviation occurs mostly on the hemisphere that is ipsilateral to the lesion. The only study that investigated the effect of ischemic stroke on connectivity gradients (Bayrak et al., 2019) also points out the fact that changes in the connectivity profile are related to the location of the lesion. An alternative explanation can be that the functional integrity of the right hemisphere is simply more fragile, and the highlighted sensitive regions are driving this hemispheric difference and behavioral deficits. The sensitive regions we reported in our study resemble the pattern of recently-discovered somato-cognitive actions network on motor cortex (Gordon et al., 2023). This network is placed on the motor cortex and acts in action planning, behaving like a bridge between mind and body. This network may be the one that suffers the most from ischemic stroke damage, therefore the patients become unable to coordinate or execute their basic motor functions.

Whether the deviation makes up for the stroke damage or is a result of it is a matter of question. In other words, the degree of deviation can indicate the degree of functional plasticity to compensate for the anatomical damage, or worse, the degree of dysfunction. The direction of the correlation between behavioral performance and the deviation can be an indicator for this question. The correlations between functional deviation and behavioral scores were almost always negative, meaning that as the behavioral performance gets better (more similar to the performance of the healthy controls), the deviation becomes smaller. This relationship can be interpreted as the deviation indicating the degree of functional deficit.

Intact and damaged hemispheres were tested separately following the previous literature on the hemispheric differences in functional connectivity after stroke (New et al., 2015; Tang et al., 2016; Urbin et al., 2014; Yourganov et al., 2021). While damaged hemispheres are similarly affected by stroke, intact hemispheres showed a lateralization effect. The right hemisphere was shown to be more sensitive to the damage on the contralateral hemisphere. In contrast, the left hemisphere is more durable and keeps its integrity better compared to the right hemisphere. Furthermore, the source of this difference is the second gradient, where the brain function is organized on the sensorimotor-visual axis. The sensitivity in the right intact hemisphere is sourced from the deviation in the regions related to the unimodal functions, and no differences related to higher-order functions are observed. In contrast to the intact hemispheres, the damaged hemispheres suffer equally in all three gradients. Lastly, damage in the right hemisphere is related to similar patterns of functional deviation, whereas damage to the left hemisphere shows

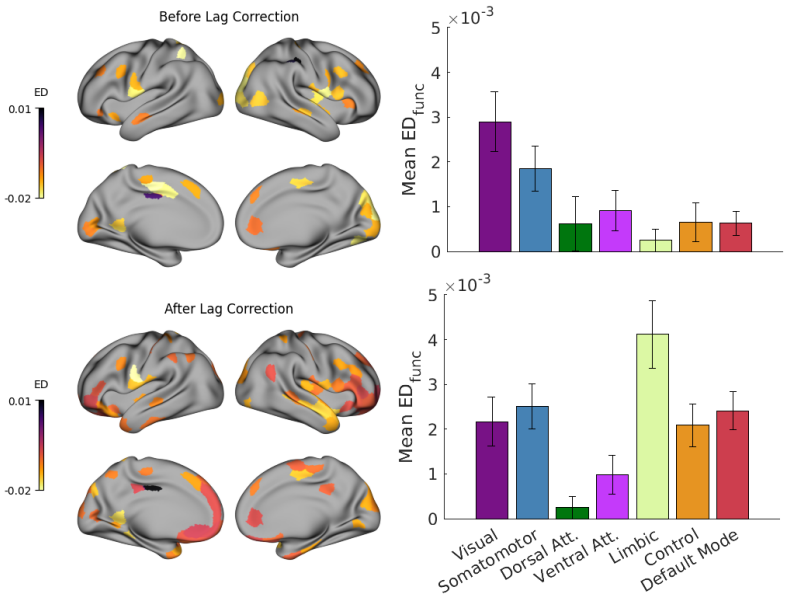

Figure 7. Impact of lag correction on the second gradient. Difference in 1D distance to the reference topography of the second gradient between groups (left) and their contribution to the 7 networks (right).ED$_{func}$ It can be seen that lag correction amplifies the difference between groups, especially in the limbic network.

no such relation. This separation supports the possible higher durability of the left hemisphere, resulting in more systematic functional reorganization in case of right hemisphere damage.

The second aim of this study was to identify the effect of temporal lag correction on the connectivity gradients. It has been reported that lag correction improves the connectivity strength for various metrics (Erdoğan et al., 2016; Siegel, Snyder, et al., 2016; Tong et al., 2019). However, to our knowledge, no study up to date investigated the influence of the lag correction on the functional connectivity gradients. Lag correction changed the gradient values for the control subject in all 3 gradients. Although the regions that show different scores vary across gradients, in all three of them, a change on the superior-inferior axis is observed. From this aspect, it can be said that time lag correction "fixes" the data on the temporal domain, decreasing the confounding effect of the blood arrival time. A similar phenomenon was observed in Erdoğan et al. (2016), where the authors reported an increased explained variance in functional connectivity after time lag correction, along with better-aligned residuals. Considering the cerebral blood circulation, which goes from inferior to superior regions, it is natural to observe differences in this axis. A similar pattern with a larger extent was revealed for stroke subjects, which means they benefited more from the correction. The difference was most prominent in the second gradient, compared to the healthy controls (Figure 6). Concordantly, the limbic network, which is located on the first end of this axis, showed the most pronounced difference after lag correction for control subjects (Figure 7). Lastly, apart from boosting the difference between intact right and left hemispheres, lag correction also improved the difference between the damaged hemispheres, resulting in a deviancy difference in the second gradient as well. Extreme lag values of stroke subjects and the increased explained variance after the correction also confirm that the time lag indicates the hemodynamic deficits of the stroke subjects. One difference that disappeared after lag correction is the similarity between functional deviation and the proximity between lesion locations. Lag correction decreased the already-low correlation between these two factors. Considering the increased differences that it was related to, it can be said the lag correction is useful to clean the data from structure-related noise for stroke subjects.

It could be expected to have a smaller difference between groups after correction since the BOLD signal is fixed to the same time domain. On the contrary, the difference is more visible. Therefore, the difference in the BOLD characteristic, at least in the time domain, can be considered as noise. Another point of view could be that the new BOLD signal after the stroke occurs may reflect the real neural activity, that happened due to plasticity and should be accepted as a whole while comparing the data between groups. For example, Siegel, Ramsey, et al. (2016) argues that although lag correction improves the connectivity, it is not suggested because there is no way to fix the other differences related to frequency. Lag correction might complicate those confounding even more. However, our findings (also theirs, Siegel, Snyder, et al., 2016) show that this is a necessary step, and the issues in the frequency domain should be handled separately. Inspiration could be drawn from the literature sudying brain tumors, were it has been found that local and global shifts of the spectrum carry prognostic Park et al. (2023) and network Falcó-Roget et al. (2024) information.

For stroke subjects, the relevance of the second gradient can be stemmed from the high similarity between the lag pattern and the second gradient. The cerebral blood flow might be driving the organization of the second gradient, which can potentially lead to a higher difference in the gradient scores of the stroke subjects after correction.

Limitations and further considerations

The number of healthy controls in the dataset remains short compared to the number of stroke subjects. Using a surface-based approach limited the ability to calculate the geodesic distance to the lesion, which could be a better indicator than the anatomical Euclidean distance. Using disconnectome maps instead of anatomical distance can increase the overall anatomical information as it was shown that it is a better estimator of stroke outcome. Special attention can be paid to the somato-cognitive action network when examining the motor cortex. In addition to correcting BOLD in the time domain, correcting the frequency domain may lead to new diagnostics and improve the data quality in the future.

Conclusions

Connectivity gradients are a valid method to examine the effect of ischemic stroke due to their low-dimensional representation of functional organization. This method highlights the sensitive regions that are placed mostly on the right hemisphere. Time lag correction is a suggested denoising method for processing fMRI data, especially if the sample includes ischemic stroke subjects. Correction of the time lag highlighted the differences between groups, especially for the second gradient.

Acknowledgments

Authors thank Prof. Maurizio Corbetta for sharing the dataset and Dr. Sophie Valk for their valuable feedback and suggestions. The publication was created within the project of the Minister of Science and Higher Education "Support for the activity of Centers of Excellence established in Poland under Horizon 2020" on the basis of the contract number MEiN/2023/DIR/3796. This project has received funding from the European Union's Horizon 2020 research and innovation programme under grant agreement No 857533. This publication is supported by Sano project carried out within the International Research Agendas programme of the Foundation for Polish Science, co-financed by the European Union under the European Regional Development Fund. This research was supported in part by the PLGrid infrastructure. Computations have been partially performed on the ARES supercomputer at ACC Cyfronet AGH

Author Contributions

Cemal Koba: Designed research, Performed research, Analyzed data, Wrote the paper. Joan Falcó-Roget: Designed research, Performed research, Wrote the paper. Alessandro Crimi: Designed research.

Data and code availabilty

The entire analysis code is at following repositories:

- https://github.com/KobaCemal/StrokeGradients
- https://github.com/JoanSano/BIDS_Constructor

Conflict of interest statement

The authors declare no conflict of interest.

References

Abraham, A., Pedregosa, F., Eickenberg, M., Gervais, P., Mueller, A., Kossaifi, J., Gramfort, A., Thirion, B., & Varoquaux, G. (2014). Machine learning for neuroimaging with scikit-learn. *Frontiers in neuroinformatics*, 14.

Altamura, C., Reinhard, M., Vry, M.-S., Kaller, C. P., Hamzei, F., Vernieri, F., Rossini, P. M., Hetzel, A., Weiller, C., & Saur, D. (2009). The longitudinal changes of bold response and cerebral hemodynamics from acute to subacute stroke. a fmri and tcd study. *BMC neuroscience*, *10*, 1–12.

Avants, B., Epstein, C., Grossman, M., & Gee, J. (2008). Symmetric diffeomorphic image registration with cross-correlation: Evaluating automated labeling of elderly and neurodegenerative brain. *Medical Image Analysis*, *12*(1), 26–41. https://doi.org/10.1016/j.media.2007.06.004

Bayrak, Ş. (2019). Stroke_preprop. https://github.com/sheyma/stroke_preprop

Bayrak, Ş., Khalil, A. A., Villringer, K., Fiebach, J. B., Villringer, A., Margulies, D. S., & Ovadia-Caro, S. (2019). The impact of ischemic stroke on connectivity gradients. *NeuroImage: Clinical*, *24*, 101947.

Bethlehem, R. A., Paquola, C., Seidlitz, J., Ronan, L., Bernhardt, B., Tsvetanov, K. A., Consortium, C.-C., et al. (2020). Dispersion of functional gradients across the adult lifespan. *Neuroimage*, *222*, 117299.

Bonakdarpour, B., Beeson, P., DeMarco, A., & Rapcsak, S. (2015). Variability in blood oxygen level dependent (bold) signal in patients with stroke-induced and primary progressive aphasia. *NeuroImage: Clinical*, *8*, 87–94.

Braban, A., Leech, R., Murphy, K., & Geranmayeh, F. (2023). Cerebrovascular reactivity has negligible contribution to hemodynamic lag after stroke: Implications for functional magnetic resonance imaging studies. *Stroke*, *54*(4), 1066–1077.

Carter, A. R., Astafiev, S. V., Lang, C. E., Connor, L. T., Rengachary, J., Strube, M. J., Pope, D. L., Shulman, G. L., & Corbetta, M. (2010). Resting interhemispheric functional magnetic resonance imaging connectivity predicts performance after stroke. *Annals of neurology*, *67*(3), 365–375.

Ciric, R., Thompson, W. H., Lorenz, R., Goncalves, M., MacNicol, E., Markiewicz, C. J., Halchenko, Y. O., Ghosh, S. S., Gorgolewski, K. J., Poldrack, R. A., et al. (2022). Templateflow: Fair-sharing of multi-scale, multi-species brain models. *bioRxiv*, 2021–02. https://doi.org/10.1101/2021.02.10.430678

Corbetta, M., Ramsey, L., Callejas, A., Baldassarre, A., Hacker, C. D., Siegel, J. S., Astafiev, S. V., Rengachary, J., Zinn, K., Lang, C. E., et al. (2015). Common behavioral clusters and subcortical anatomy in stroke. *Neuron*, *85*(5), 927–941.

Corbetta, M., & Shulman, G. L. (2002). Control of goal-directed and stimulus-driven attention in the brain. *Nature reviews neuroscience*, *3*(3), 201–215.

Cox, R. W., & Hyde, J. S. (1997). Software tools for analysis and visualization of fmri data. *NMR in Biomedicine*, *10*(4-5), 171–178. https://doi.org/10.1002/(SICI)1099-1492(199706/08)10:4/5<171::AID-NBM453>3.0.CO;2-L

Del Río, M., Racey, C., Ren, Z., Qiu, J., Wang, H.-T., & Ward, J. (2022). Higher sensory sensitivity is linked to greater expansion amongst functional connectivity gradients. *Journal of Autism and Developmental Disorders*, 1–19.

Erdoğan, S. B., Tong, Y., Hocke, L. M., Lindsey, K. P., & deB Frederick, B. (2016). Correcting for blood arrival time in global mean regression enhances functional connectivity analysis of resting state fmri-bold signals. *Frontiers in human neuroscience*, *10*, 311.

Esteban, O., Blair, R., Markiewicz, C. J., Berleant, S. L., Moodie, C., Ma, F., Isik, A. I., Erramuzpe, A., Kent, M., James D. andGoncalves, DuPre, E., Sitek, K. R., Gomez, D. E. P., Lurie, D. J., Ye, Z., Poldrack, R. A., & Gorgolewski, K. J. (2018). Fmriprep. *Software*. https://doi.org/10.5281/zenodo.852659

Esteban, O., Markiewicz, C., Blair, R. W., Moodie, C., Isik, A. I., Erramuzpe Aliaga, A., Kent, J., Goncalves, M., DuPre, E., Snyder, M., Oya, H., Ghosh, S., Wright, J., Durnez, J., Poldrack, R., & Gorgolewski, K. J. (2019). fMRIPrep: A robust preprocessing pipeline for functional MRI. *Nature Methods*, *16*, 111–116. https://doi.org/10.1038/s41592-018-0235-4

Falcó-Roget, J. (2023). Bids converter. https://github.com/JoanSano/BIDS_Constructor

Falcó-Roget, J., Cacciola, A., Sambataro, F., & Crimi, A. (2024). Functional and structural reorganization in brain tumors: A machine learning approach using desynchronized functional oscillations. *Communications Biology*, *7*(1), 419. https://doi.org/https://doi.org/10.1038/s42003-024-06119-3

Fonov, V., Evans, A., McKinstry, R., Almli, C., & Collins, D. (2009). Unbiased nonlinear average age-appropriate brain templates from birth to adulthood. *NeuroImage*, *47, Supplement 1*, S102. https://doi.org/10.1016/S1053-8119(09)70884-5

Gale, D., de Wael, R. V., Benkarim, O., Bernhardt, B., et al. (2021). Surfplot: Publication-ready brain surface figures. *Zenodo*.

Glen, D., Reynolds, R., Taylor, P., You, X., Kong, R., Xue, A., Yan, X., & Yeo, B. (2021). Improved rois with afni+ suma processing. *27th annual meeting of the Organization for Human Brain Mapping, Poster*, *1672*.

Gordon, E. M., Chauvin, R. J., Van, A. N., Rajesh, A., Nielsen, A., Newbold, D. J., Lynch, C. J., Seider, N. A., Krimmel, S. R., Scheidter, K. M., et al. (2023). A somato-cognitive action network alternates with effector regions in motor cortex. *Nature*, 1–9.

Gorgolewski, K., Burns, C. D., Madison, C., Clark, D., Halchenko, Y. O., Waskom, M. L., & Ghosh, S. (2011). Nipype: A flexible, lightweight and extensible neuroimaging data processing framework in python. *Frontiers in Neuroinformatics*, *5*, 13. https://doi.org/10.3389/fninf.2011.00013

Gorgolewski, K. J., Esteban, O., Markiewicz, C. J., Ziegler, E., Ellis, D. G., Notter, M. P., Jarecka, D., Johnson, H., Burns, C., Manhães-Savio, A., Hamalainen, C., Yvernault, B., Salo, T., Jordan, K., Goncalves, M., Waskom, M., Clark, D., Wong, J., Loney, F., … Ghosh, S. (2018). Nipype. *Software*. https://doi.org/10.5281/zenodo.596855

Gratton, C., Nomura, E. M., Pérez, F., & D'Esposito, M. (2012). Focal brain lesions to critical locations cause widespread disruption of the modular organization of the brain. *Journal of cognitive neuroscience*, *24*(6), 1275–1285.

Greve, D. N., & Fischl, B. (2009). Accurate and robust brain image alignment using boundary-based registration. *NeuroImage*, *48*(1), 63–72. https://doi.org/10.1016/j.neuroimage.2009.06.060

Hardikar, S., Mckeown, B., Schaare, H. L., Xu, T., Lauckner, M. E., Valk, S. L., Margulies, D. S., Turnbull, A., Bernhardt, B., Vos de Wael, R., et al. (2022). Macro-scale patterns in functional connectivity associated with ongoing thought patterns and dispositional traits. *bioRxiv*, 2022–10.

He, B. J., Snyder, A. Z., Vincent, J. L., Epstein, A., Shulman, G. L., & Corbetta, M. (2007). Breakdown of functional connectivity in frontoparietal networks underlies behavioral deficits in spatial neglect. *Neuron*, *53*(6), 905–918.

Hong, J. M., Kim, D. S., & Kim, M. (2021). Hemorrhagic transformation after ischemic stroke: Mechanisms and management. *Frontiers in Neurology*, *12*, 703258.

Hong, S.-J., Vos de Wael, R., Bethlehem, R. A., Lariviere, S., Paquola, C., Valk, S. L., Milham, M. P., Di Martino, A., Margulies, D. S., Smallwood, J., et al. (2019). Atypical functional connectome hierarchy in autism. *Nature communications*, *10*(1), 1022.

Jenkinson, M., Bannister, P., Brady, M., & Smith, S. (2002). Improved optimization for the robust and accurate linear registration and motion correction of brain images. *NeuroImage*, *17*(2), 825–841. https://doi.org/10.1006/nimg.2002.1132

Jenkinson, M., & Smith, S. (2001). A global optimisation method for robust affine registration of brain images. *Medical Image Analysis*, *5*(2), 143–156. https://doi.org/10.1016/S1361-8415(01)00036-6

Khalil, A. A., Villringer, K., Filleböck, V., Hu, J.-Y., Rocco, A., Fiebach, J. B., & Villringer, A. (2020). Non-invasive monitoring of longitudinal changes in cerebral hemodynamics in acute ischemic stroke using bold signal delay. *Journal of Cerebral Blood Flow & Metabolism*, *40*(1), 23–34.

Kurtzer, G. M., Sochat, V., & Bauer, M. W. (2017). Singularity: Scientific containers for mobility of compute. *PloS one*, *12*(5), e0177459.

Lanczos, C. (1964). Evaluation of noisy data. *Journal of the Society for Industrial and Applied Mathematics Series B Numerical Analysis*, *1*(1), 76–85. https://doi.org/10.1137/0701007

Lv, Y., Margulies, D. S., Cameron Craddock, R., Long, X., Winter, B., Gierhake, D., Endres, M., Villringer, K., Fiebach, J., & Villringer, A. (2013). Identifying the perfusion deficit in acute stroke with resting-state functional magnetic resonance imaging. *Annals of neurology*, *73*(1), 136–140.

Margulies, D. S., Ghosh, S. S., Goulas, A., Falkiewicz, M., Huntenburg, J. M., Langs, G., Bezgin, G., Eickhoff, S. B., Castellanos, F. X., Petrides, M., et al. (2016). Situating the default-mode network along a principal gradient of macroscale cortical organization. *Proceedings of the National Academy of Sciences*, *113*(44), 12574–12579.

Mckeown, B., Strawson, W. H., Wang, H.-T., Karapanagiotidis, T., de Wael, R. V., Benkarim, O., Turnbull, A., Margulies, D., Jefferies, E., McCall, C., et al. (2020). The relationship between individual variation in macroscale functional gradients and distinct aspects of ongoing thought. *NeuroImage*, *220*, 117072.

New, A. B., Robin, D. A., Parkinson, A. L., Duffy, J. R., McNeil, M. R., Piguet, O., Hornberger, M., Price, C. J., Eickhoff, S. B., & Ballard, K. J. (2015). Altered resting-state network connectivity in stroke patients with and without apraxia of speech. *NeuroImage: Clinical*, *8*, 429–439.

Park, K. Y., Snyder, A. Z., Olufawo, M., Trevino, G., Luckett, P. H., Lamichhane, B., Xie, T., Lee, J. J., Shimony, J. S., & Leuthardt, E. C. (2023). Glioblastoma induces whole-brain spectral change in resting state fmri: Associations with clinical comorbidities and overall survival. *NeuroImage: Clinical*, *39*, 103476. https://doi.org/https://doi.org/10.1016/j.nicl.2023.103476

Power, J. D., Mitra, A., Laumann, T. O., Snyder, A. Z., Schlaggar, B. L., & Petersen, S. E. (2014). Methods to detect, characterize, and remove motion artifact in resting state fmri. *NeuroImage*, *84*(Supplement C), 320–341. https://doi.org/10.1016/j.neuroimage.2013.08.048

Rehme, A. K., Fink, G. R., Von Cramon, D. Y., & Grefkes, C. (2011). The role of the contralesional motor cortex for motor recovery in the early days after stroke assessed with longitudinal fmri. *Cerebral cortex*, *21*(4), 756–768.

Roach, E. S., Bettermann, K., & Biller, J. (2010). Pathophysiology of ischemic stroke. In *Toole's cerebrovascular disorders* (pp. 60–74). Cambridge University Press.

Satterthwaite, T. D., Elliott, M. A., Gerraty, R. T., Ruparel, K., Loughead, J., Calkins, M. E., Eickhoff, S. B., Hakonarson, H., Gur, R. C., Gur, R. E., & Wolf, D. H. (2013). An improved framework for confound regression and filtering for control of motion artifact in the preprocessing of resting-state functional connectivity data. *NeuroImage*, *64*, 240–256. https://doi.org/10.1016/j.neuroimage.2012.08.052

Schaefer, A., Kong, R., Gordon, E. M., Laumann, T. O., Zuo, X.-N., Holmes, A. J., Eickhoff, S. B., & Yeo, B. T. T. (2018). Local-Global Parcellation of the Human Cerebral Cortex from Intrinsic Functional Connectivity MRI. *Cerebral Cortex (New York, N.Y.: 1991)*, *28*(9), 3095–3114. https://doi.org/10.1093/cercor/bhx179

Siegel, J. S., Snyder, A. Z., Ramsey, L., Shulman, G. L., & Corbetta, M. (2016). The effects of hemodynamic lag on functional connectivity and behavior after stroke. *Journal of Cerebral Blood Flow & Metabolism*, *36*(12), 2162–2176.

Siegel, J. S., Ramsey, L. E., Snyder, A. Z., Metcalf, N. V., Chacko, R. V., Weinberger, K., Baldassarre, A., Hacker, C. D., Shulman, G. L., & Corbetta, M. (2016). Disruptions of network connectivity predict impairment in multiple behavioral domains after stroke. *Proceedings of the National Academy of Sciences*, *113*(30), E4367–E4376.

Tang, C., Zhao, Z., Chen, C., Zheng, X., Sun, F., Zhang, X., Tian, J., Fan, M., Wu, Y., & Jia, J. (2016). Decreased functional connectivity of homotopic brain regions in chronic stroke patients: A resting state fmri study. *PloS one*, *11*(4), e0152875.

Thiebaut de Schotten, M., Foulon, C., & Nachev, P. (2020). Brain disconnections link structural connectivity with function and behaviour. *Nature communications*, *11*(1), 5094.

Tong, Y., Hocke, L. M., & Frederick, B. B. (2019). Low frequency systemic hemodynamic "noise" in resting state bold fmri: Characteristics, causes, implications, mitigation strategies, and applications. *Frontiers in neuroscience*, *13*, 787.

Tong, Y., Lindsey, K. P., Hocke, L. M., Vitaliano, G., Mintzopoulos, D., & Frederick, B. d. (2017). Perfusion information extracted from resting state functional magnetic resonance imaging. *Journal of Cerebral Blood Flow & Metabolism*, *37*(2), 564–576.

Tustison, N. J., Avants, B. B., Cook, P. A., Zheng, Y., Egan, A., Yushkevich, P. A., & Gee, J. C. (2010). N4itk: Improved n3 bias correction. *IEEE Transactions on Medical Imaging*, *29*(6), 1310–1320. https://doi.org/10.1109/TMI.2010.2046908

Urbin, M., Hong, X., Lang, C. E., & Carter, A. R. (2014). Resting-state functional connectivity and its association with multiple domains of upper-extremity function in chronic stroke. *Neurorehabilitation and neural repair*, *28*(8), 761–769.

Valk, S. L., Kanske, P., Park, B.-y., Hong, S.-J., Böckler, A., Trautwein, F.-M., Bernhardt, B. C., & Singer, T. (2023). Functional and microstructural plasticity following social and interoceptive mental training. *Elife*, *12*, e85188.

Vos de Wael, R., Benkarim, O., Paquola, C., Lariviere, S., Royer, J., Tavakol, S., Xu, T., Hong, S.-J., Langs, G., Valk, S., et al. (2020). Brainspace: A toolbox for the analysis of macroscale gradients in neuroimaging and connectomics datasets. *Communications biology*, *3*(1), 103.

Weaver, N. A., Zhao, L., Biesbroek, J. M., Kuijf, H. J., Aben, H. P., Bae, H.-J., Caballero, M. Á., Chappell, F. M., Chen, C. P., Dichgans, M., et al. (2019). The meta vci map consortium for meta-analyses on strategic lesion locations for vascular cognitive impairment using lesion-symptom mapping: Design and multicenter pilot study. *Alzheimer's & Dementia: Diagnosis, Assessment & Disease Monitoring*, *11*(1), 310–326.

Worsley, K. J., Taylor, J., Carbonell, F., Chung, M., Duerden, E., Bernhardt, B., Lyttelton, O., Boucher, M., Evans, A., et al. (2009). A matlab toolbox for the statistical analysis of univariate and multivariate surface and volumetric data using linear mixed effects models and random field theory. *NeuroImage Organisation for Human Brain Mapping 2009 Annual Meeting*, *47*, S102.

Xia, M., Liu, J., Mechelli, A., Sun, X., Ma, Q., Wang, X., Wei, D., Chen, Y., Liu, B., Huang, C.-C., et al. (2022). Connectome gradient dysfunction in major depression and its association with gene expression profiles and treatment outcomes. *Molecular Psychiatry*, *27*(3), 1384–1393.

Yourganov, G., Stark, B. C., Fridriksson, J., Bonilha, L., & Rorden, C. (2021). Effect of stroke on contralateral functional connectivity. *Brain Connectivity*, *11*(7), 543–552.

Zhang, Y., Brady, M., & Smith, S. (2001). Segmentation of brain MR images through a hidden markov random field model and the expectation-maximization algorithm. *IEEE Transactions on Medical Imaging*, *20*(1), 45–57. https://doi.org/10.1109/42.906424

Zhu, Y., Bai, L., Liang, P., Kang, S., Gao, H., & Yang, H. (2017). Disrupted brain connectivity networks in acute ischemic stroke patients. *Brain imaging and behavior*, *11*, 444–453.

Supplementary Material: Effect of acute ischemic stroke on functional connectivity gradients

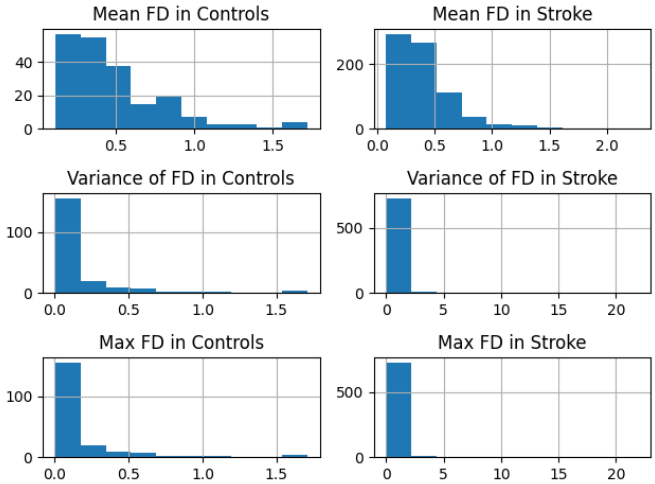

Supplementary Figure 1. Comparison of FD values between control and stroke subjects.

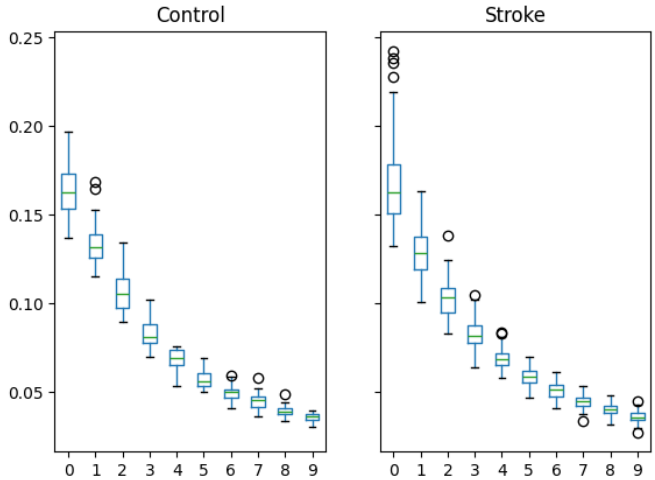

Supplementary Figure 2. Scaled eigenvalues of the 10 gradients for control and stroke subjects.

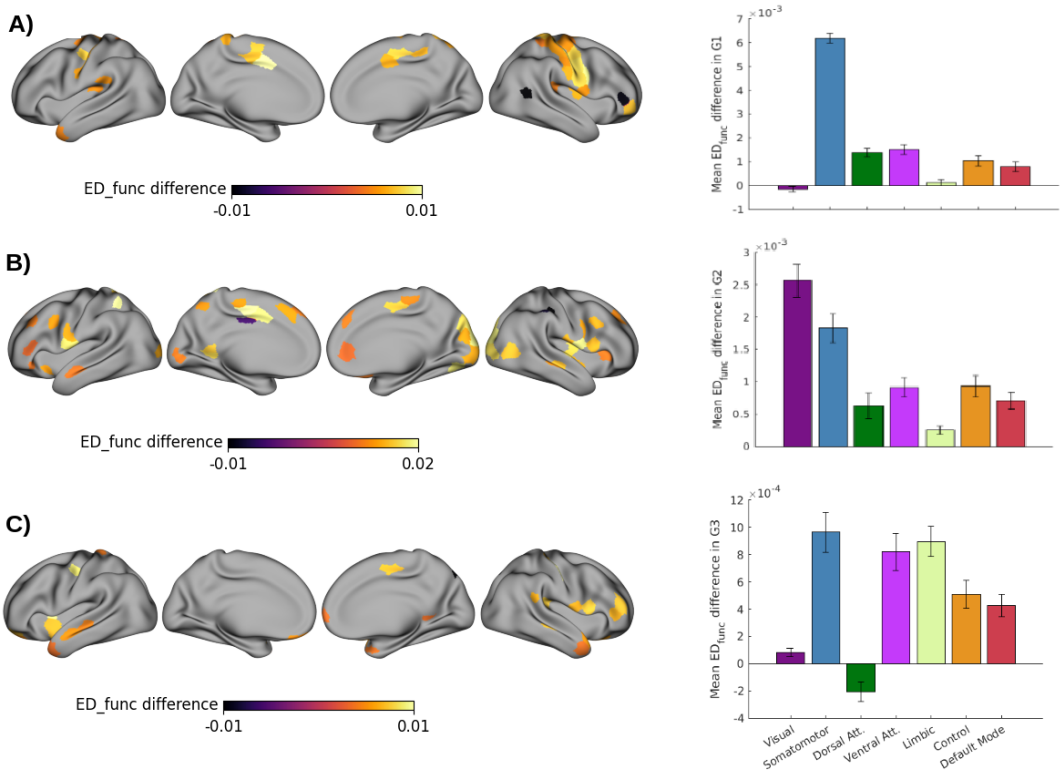

Supplementary Figure 3. ED_{func} differences between control and stroke subjects and their network decompositions across gradients. **A)** G1, **B)** G2, **C)** G3.

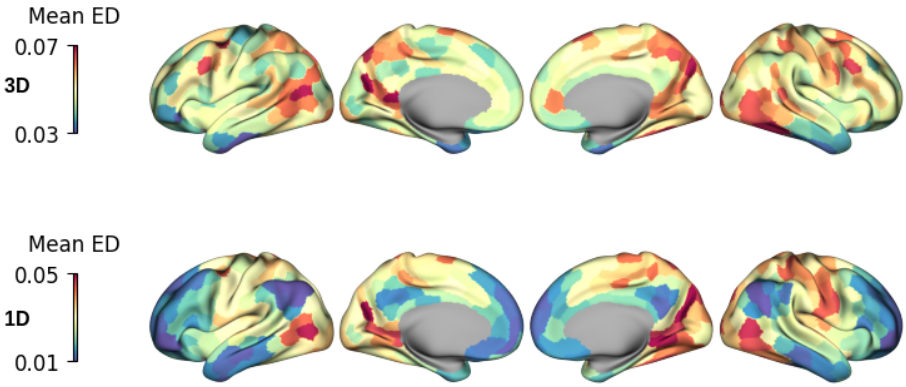

Supplementary Figure 4. Mean 3D and 1D distance of the intact hemispheres. It can be seen that the the highest difference on the 2nd gradient is placed on the visual and sensorimotor areas.

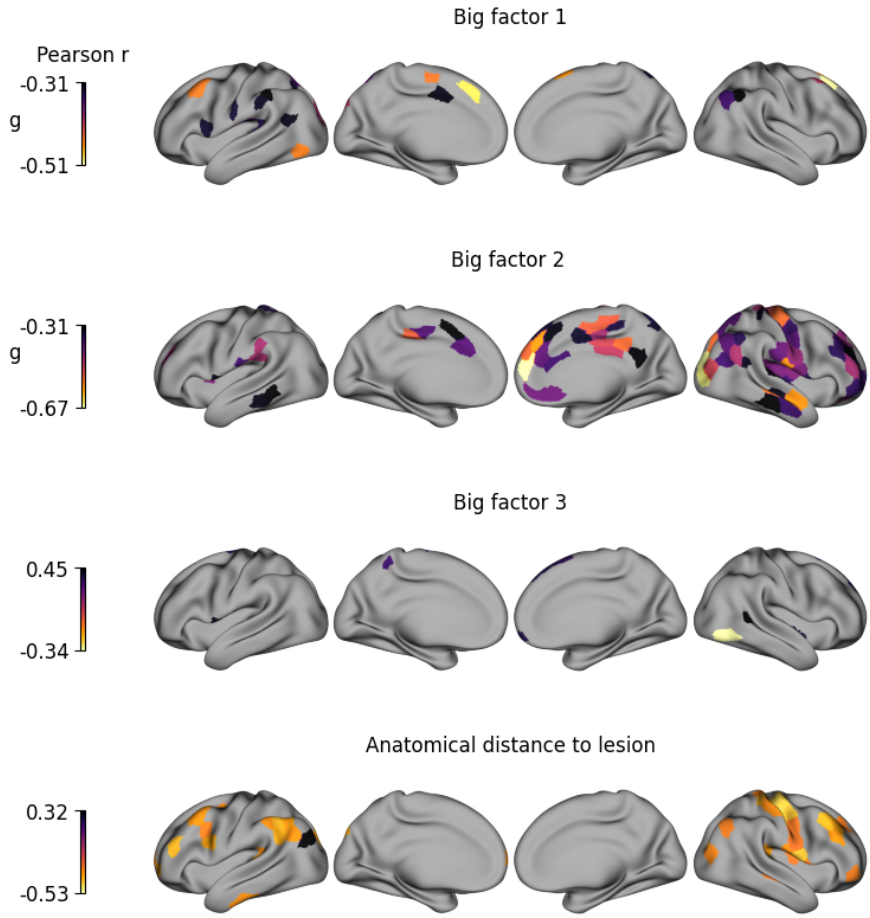

Supplementary Figure 5. Behavioral and structural correlates of ED_{func} ($p < 0.05$, not corrected via multiple comparison correction procedures)

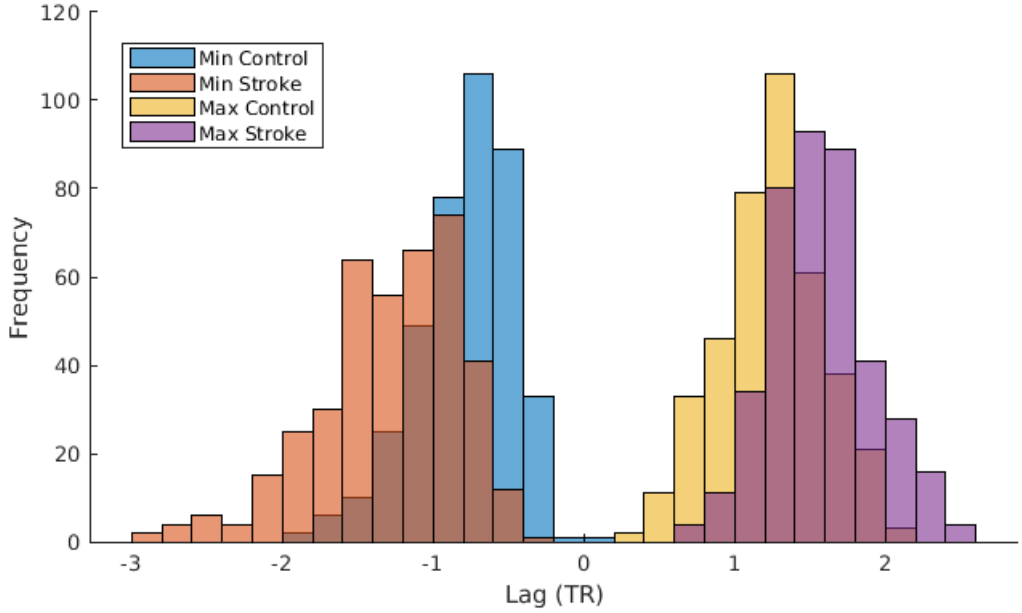

Supplementary Figure 6. Minimum and maximum lag values of control and stroke subjects.